Hydrogen sulfide-releasing nanocascade templated by glucose oxidase for diabetic infection treatment

*Yuxuan Ge, Fan Rong, Yujia Lu, Zixin Wang, Jinyu Liu, Junsheng Chen, Wei Li, and Yin Wang**

Engineering Research Center of Cell & Therapeutic Antibody, School of Pharmacy, Shanghai Jiao Tong University, Shanghai 200240, China
E-mail: yinwang@sjtu.edu.cn

Keywords: hydrogen sulfide, Fenton-like reaction, diabetic infection, glucose oxidase

Diabetic ulcer receives much attention in recent years due to its high incidence and mortality, promoting the scientific community to develop various strategies for such chronic disease treatments. However, the therapeutic outcome of these approaches is highly compromised by the invasive bacteria and severe inflammatory ulcer microenvironment. To overcome these dilemmas, microenvironment-responsive self-delivery GOx@MnS nanoparticles (NPs) are developed by a one-step biomineralization. When encountered with high glucose level in the ulcer site, GOx catalyze glucose to decrease the local pH and trigger the steady release of both manganese ions (Mn^{2+}) and hydrogen sulfide (H_2S). Mn^{2+} react with hydrogen peroxide to generate hydroxyl radical for the elimination of bacterial infection, meanwhile H_2S is able to suppress the inflammatory response and accelerate diabetic wound healing through macrophage polarization. The excellent biocompatibility, strong bactericidal activity, and considerable immunomodulatory effect promise GOx@MnS NPs great therapeutic potential for diabetic wound treatment.

1. Introduction

Diabetes mellitus (DM) remains one of the most common chronic metabolic diseases over the world.[1] DM patients suffer from various complications, such as diabetic ulcer, due to hyperglycemia-induced systemic neuropathy and vasculopathy.[2] Chronic inflammation and

hypoxic microenvironment caused by vasculopathy hinder the fast skin regeneration, meanwhile high glucose level in tissue fluid provides a hotbed for bacterial infection. Once infection occurs, bacteria resided in the wound aggravate the tissue damage and prevent the diabetic wound from steadily healing, which further result in severer ulcer or even necrosis. Consequently, diabetic wound is usually hard to heal and has become a major healthcare issue nowadays.[3] In clinic, treatments for such chronically infected wound generally employ antibiotics and hypoglycemic agents, nevertheless the therapeutic outcome is highly compromised by fluctuated glycemic level and various types of multi-drug resistant bacteria in wound.[4] Therefore, development of anti-bacterial and anti-inflammation strategy directing toward diabetic wounds is highly needed.

In the past few years, various materials capable of eliminating diabetic infection has been constructed.[5] Unlike conventional antibiotics, anti-bacterial materials generally utilize the specific microenvironment of diabetic infection to evoke the efficacy. For instance, a fungi-sourced natural enzyme, glucose oxidase (GOx), has been frequently selected to fabricate anti-bacterial nanomaterials, because GOx can catalyze *D*-glucose to generate hydrogen peroxide (H_2O_2) as well as gluconic acid under aerobic condition.[6] The catalytic process depletes excess glucose and reconstitutes the weak acidic microenvironment, meanwhile forming reactive oxygen species (ROS) to kill bacteria. However, in fact, GOx itself is not an ideal anti-bacterial agent for diabetic infection. Although *in situ* generation of H_2O_2 in a low concentration avoids to damage normal tissues, it also somehow attenuates the bactericidal activity. The practical strategy to enhance its bactericidal activity may rely on generation of ROS with stronger oxidizing property, such as hydroxyl radical (•OH), through cascade reaction.[7] Various catalysts, including natural enzyme (e.g., horseradish peroxidase),[8] metal nanozyme (e.g., platinum nanozyme),[9] and transition metal ions (e.g., ferrous ion),[10] have been synergized with GOx to facilitate the cascade reaction and cure diabetic infection. Powered by •OH generating cascade, these catalytic materials gain extremely strong and broad-spectrum bactericidal activity without inducing potential drug resistance, which gratifyingly breaks the limitations of antibiotics. Nevertheless, these GOx-based nanomaterials offer meagre effect

either on alleviating inflammatory response or promoting tissue regeneration, implying that their therapeutic efficacy may not be powerful enough against severe ulcer. In this regard, incorporation of an appropriate anti-inflammatory reagent to synergize GOx-based nanomaterials would be a smart strategy for diabetic wound treatment.

Owing to the inherent physiologically modulating effects, gasotransmitter-based strategy has become an emerging field for wound treatment.[11] Among them, hydrogen sulfide (H_2S) participates in various vital processes associated with wound healing, including inflammatory suppression, endothelial cell proliferation, and angiogenesis, through a dose-dependent manner.[12] Notably, H_2S could exert anti-inflammatory effect at physiological concentration without obvious side effects. This is quite different from steroid hormones, the anti-inflammatory agent commonly used in clinic that may cause endocrine dyscrasia in DM patients.[13] On account of these merits, H_2S could be an ideal agent for diabetic wounds treatment through the integrated anti-inflammation and pro-healing effects. However, the therapeutic efficacy of H_2S on infected diabetic wound is hindered by the uncontrolled release behavior. Therefore, a well-designed stimuli-responsive system enabling on-demand H_2S release kinetics is of great importance, so as to maintain therapeutic efficacy and avoid potential side effects.[14] Recently, water-insoluble metal sulfides (manganese sulfide (MnS) and zinc sulfide (ZnS), etc.) are well explored for therapeutic H_2S delivery.[15] In these cases, through the simple biomineralization method, metal sulfide nanocomposites could be fabricated templated by certain biomacromolecules. Upon encountering with the pathological microenvironment, H_2S and functional metal ions would be unleashed for the synergistic or cascade therapy. To the best of our knowledge, there is no report on H_2S-releasing nanocascade templated by glucose oxidase for diabetic wound treatment.

Herein, we reported on the construction of a self-delivery, H_2S-liberating nanocascade for infected diabetic wound treatment. GOx was selected as the "carrier" of the composite, and water-insoluble H_2S donor MnS was deposited on the surface of GOx by *in situ* biomineralization to afford GOx@MnS nanoparticles (NPs) without any other stabilizer. In

addition, GOx served as the "promotor" of the cascade therapeutic activity. As the enzymatic activity of GOx could be well preserved after biomineralization, GOx catalyzed glucose in fluid to generate gluconic acid and H_2O_2 when spread on wound surface.[16] On one hand, gluconic acid reduced the environmental pH to trigger H_2S release from MnS. On the other hand, H_2O_2 could be persistently transformed into •OH through Mn^{2+}-catalyzed Fenton-like reaction.[17] Once generated at wound surface, •OH could rapidly kill the resided bacteria via breaking their cytoderm. More importantly, its high chemical reactivity but short half-life limits its action to bacteria and tissues on the surface only, alleviating the potential damage to deep areas. Hence, GOx@MnS NPs offer a perceptive combination of glucose - H_2O_2 - •OH cascade and H_2S donor for diabetic infection treatment (Scheme 1).

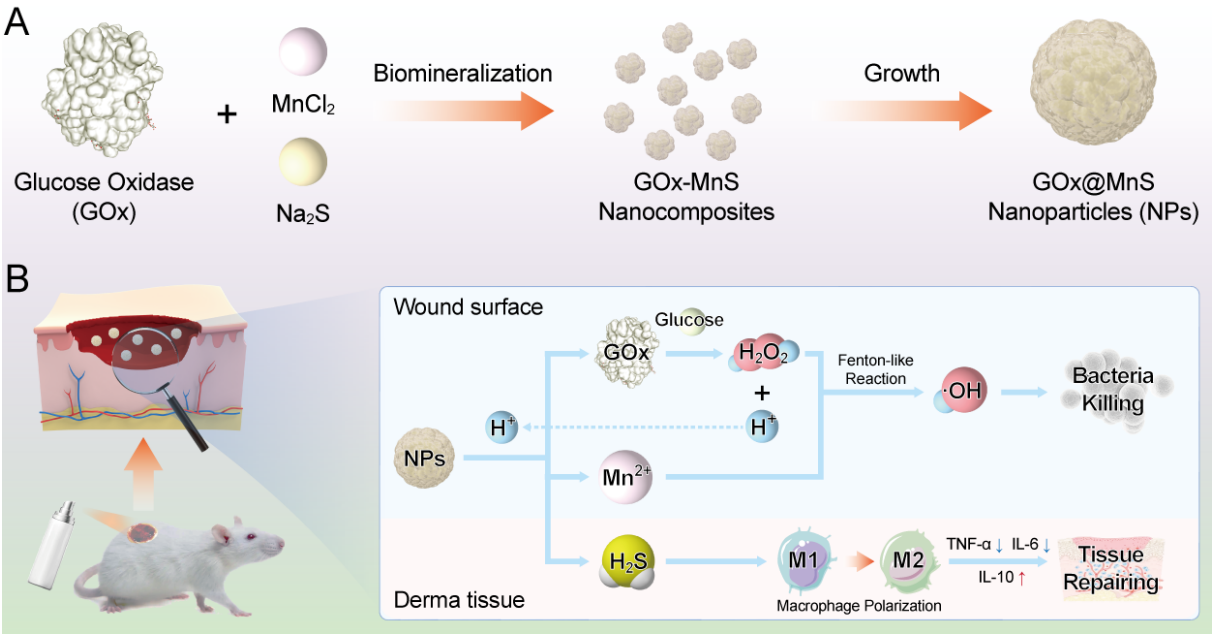

Scheme 1. A schematic diagram of GOx@MnS NPs for diabetic wound treatment. (A) Synthesis of GOx@MnS NPs by *in situ* biomineralization. (B) When spread on diabetic wound surface, GOx@MnS NPs catalyzed glucose into gluconic acid and H_2O_2, which in turn decomposed into free GOx, Mn^{2+}, and H_2S. Mn^{2+} catalyzed H_2O_2 to form •OH through Fenton-like reaction for bacterial killing, meanwhile H_2S induced macrophage polarization to accelerate tissue regeneration.

2. Results and Discussion

The synthesis of GOx@MnS NPs followed a single-step biomineralization method. Briefly, manganese chloride ($MnCl_2$) was slowly added to the pre-mixed aqueous solution of GOx and sodium sulfide (Na_2S) under a neutral and anaerobic condition. GOx is an acidic protein with isoelectric points ranged from pH 3.9 to 4.3, which enables GOx to possess a strong negative charged surface in the neutral condition for Mn^{2+} adsorption.[18] As a consequence, the insoluble MnS crystal was firstly *in situ* deposited on the surface of GOx, and then the spherical NPs with coarse surface were formed through the further growth and aggregation (Figure 1A). Energy dispersive spectroscopy (EDS) mapping in Figure 1B verified the existence of C, N, O, S, and Mn in NPs. And these elements uniformly distributed within the spherical structures, indicating that the NPs were the congeries of many small MnS-GOx nanocomposites. Compared with irregularly shaped bare MnS (Figure S1), the addition of GOx in the synthetic procedure greatly optimized the morphology. The average hydrodynamic size of NPs detected by the dynamic light scattering (DLS) was 164.7 nm with an ultra-small polydispersity index (PDI) of 0.078 (Figure 1C). The surface ζ-potential was measured to be -26.3 mV (Figure S2), promising good colloidal stability in aqueous solutions. Then, the crystalline structure of the NPs was characterized by X-ray powder diffraction (XRD). The pattern demonstrated that the MnS within NPs was γ-phase (ICDD PDF# 00-040-1289) (Figure 1D). Thus, it can be deduced the light brown appearance of dried NPs powder (Figure S3) was composed of pink γ-MnS crystal and yellowish GOx. X-ray photoelectron spectroscopy (XPS) analysis also proved the existence of MnS in NPs (Figure 1E and Figure S4). Taken together, spherical GOx@MnS NPs were successfully synthesized by the *in situ* one-step biomineralization.

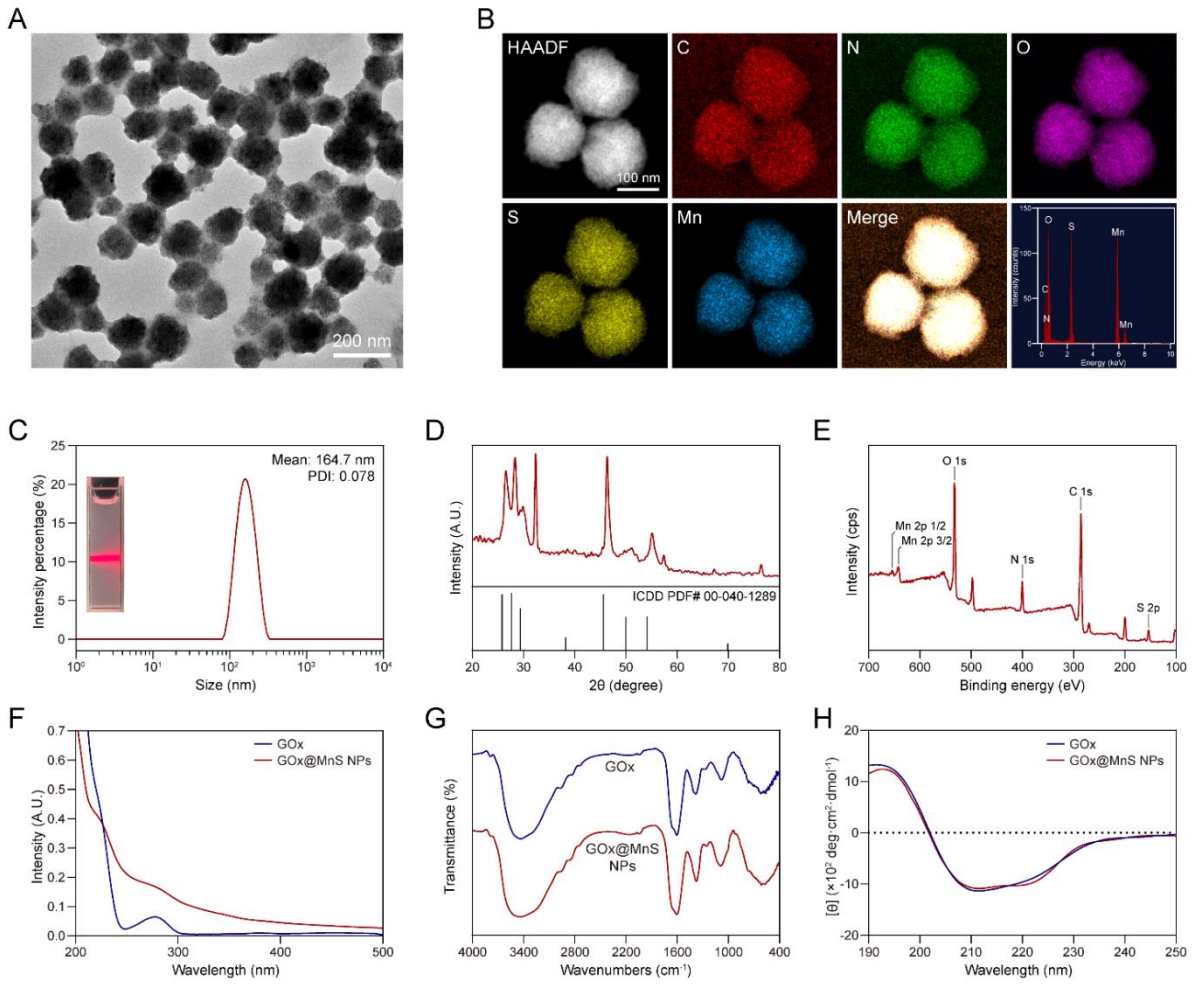

Figure 1. Characterization of GOx@MnS NPs. (A) Representative transmission electron microscope (TEM) image of GOx@MnS NPs. (B) Elemental mapping and EDS spectrum of GOx@MnS NPs (HAADF: high-angle annular dark field). (C) Hydrodynamic size distribution and Tyndall effect of GOx@MnS NPs in deionized water. (D) XRD pattern of GOx@MnS NPs compared with standard γ-phase MnS. (E) XPS spectrum of GOx@MnS NPs. (F) UV-vis spectra of free GOx and GOx@MnS NPs. (G) FT-IR spectra of free GOx and GOx@MnS NPs. (H) CD spectra of free GOx and GOx@MnS NPs in deionized water. The concentration of GOx and GOx@MnS NPs was 25 μg / mL, and 50 μg / mL, respectively.

GOx contains two flavin adenine dinucleotide (FAD) prosthetic groups for electron transport.[19] Unlike ferroheme-assisted oxidoreductases (e.g., cytochrome C oxidase), FAD-assisted GOx is tolerant to H_2S treatment in theory,[20] which offers the opportunity for sulfide deposition and the deposition process would have a negligible influence on protein structure

and enzymatic activity. After biomineralization, UV-vis spectrum of NPs displayed the characteristic absorption bands of GOx at ~280 nm (Figure 1F), meanwhile FT-IR spectrum of NPs was approximately the same as that of free GOx (Figure 1G), both indicating that GOx did not change much within NPs. Besides, we checked the content of GOx (49.98 ± 6.94 %) via Bradford assay, and, notably, the inherent fluorescence of GOx at ~350 nm (contributed by tryptophan residuals) was significantly suppressed after biomineralization due to the occurrence of aggregation-caused quenching (Figure S5). These data again confirmed the successful construction of GOx@MnS NPs. Moreover, no remarkable change of NPs in α-helix secondary structure was observed in circular dichroism (CD) spectrum compared with that of free GOx (Figure 1H). Thus, we could preliminarily conjecture that GOx did not have any significant alteration in structure during the biomineralized process. And GOx could not only work as a template for MnS deposition during the preparation process but also as a bioactive ingredient in this system (see detailed discussion below).

Subsequently, the activities of GOx@MnS NPs as an H_2S donor and cascade catalyst were tested. As indicated before, γ-MnS can be considered as a pH-responsive H_2S donor because it was insoluble in neutral or alkaline condition but slightly soluble in weak acidic condition.[15a] Thus, the release behaviors of H_2S from GOx@MnS NPs were examined in acetate buffer at pH = 7.4 and 5.5, respectively. As shown in Figure 2A, traceable amount of H_2S release from 50 μg / mL of GOx@MnS NPs was observed in neutral aqueous solution. In sharp contrast, when the pH value was lowered to 5.5, steady release of H_2S lasted up to 1 h, and the peaking concentration reached to 73 μM. Meanwhile, the enzymatic activity of GOx in the NPs was also investigated by detection of gluconic acid and H_2O_2 formation with different incubation time (0 - 4 h) and glucose level (0 - 10 mM). The test on pH decline showed that both free GOx and NPs could significantly reduce the pH, and the pH reducing extent was positively related with incubation time (Figure S7) and glucose concentration (Figure 2B). Likewise, H_2O_2 generation also followed the same trend, where longer incubation time or higher glucose level led to higher H_2O_2 level (Figure S9 and Figure 2C). Although some GOx was encapsulated inside the core of NPs, the one distributed on the surface could still initiate the oxidation of

glucose and produce acid for subsequent reactions. Consequently, the enzymatic activity of biomineralized GOx was negligibly affected. It should be noted that biomineralized NPs exhibited good stability, i.e., both the average particle size and enzymatic activity of GOx were not significantly fluctuated in 5 days when stored at 4 °C (Figure 2D). Consistent with our hypothesis, all these results above affirmed that the activity of GOx was well-preserved in GOx@MnS NPs.

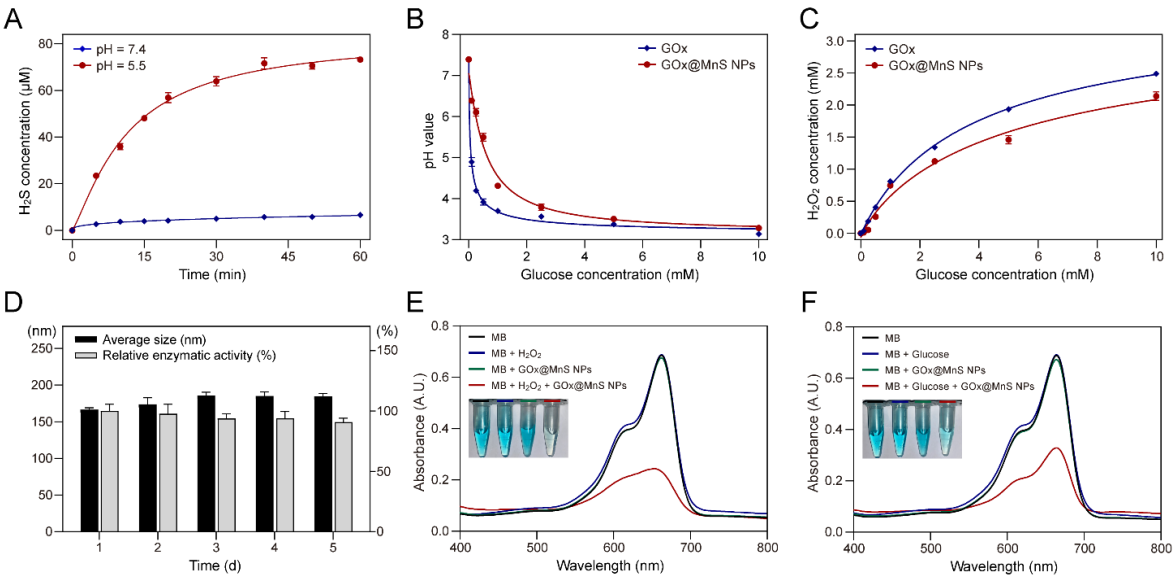

Figure 2. H_2S release behaviors and the catalytic activity of GOx@MnS NPs. (A) H_2S release curves of GOx@MnS NPs in 25 mM acetate buffer at 37 °C (pH = 7.4 or 5.5). The concentration of GOx@MnS NPs was 50 μg / mL. (B) pH declines and (C) H_2O_2 generation in GOx@MnS NPs solution with different concentration of glucose for 4 h. The concentration of GOx and GOx@MnS NPs was 25 μg / mL, and 50 μg / mL, respectively. (D) Stability of particle size and enzymatic activity over 5 days in deionized water. The solution was stored at 4 °C. (E) UV-vis spectra and the representative image of MB degradation after treated with H_2O_2 and / or GOx@MnS NPs for 2 h. The concentration of H_2O_2 was 10 mM, GOx@MnS NPs was 50 μg / mL, MB was 10 μg / mL, and $NaHCO_3$ was 25 mM for all groups. (F) UV-vis spectra and the representative image of MB degradation treated with glucose and / or GOx@MnS NPs for 2 h. The concentration of glucose was 10 mM, GOx@MnS NPs was 50 μg / mL, MB was 10 μg / mL, and $NaHCO_3$ was 25 mM for all groups.

As H_2S release from GOx@MnS NPs in weak acidic condition accompanied by the liberation of manganese (II) ions, the Fenton-like reaction between Mn^{2+} and H_2O_2 was then studied. Methylene blue (MB) was used to indicate the generation of •OH, whose absorbance at ~660 nm would decrease upon being oxidized by •OH. As shown in Figure 2E, when H_2O_2 was added into the NPs solution, •OH generated from the Fenton-like reaction could remarkably decrease the absorbance of MB and fade its color. However, incubation MB with NPs or H_2O_2 alone did not show any noticeable change. Similar results were also obtained after replacing H_2O_2 with glucose (Figure 2F). Although glucose itself would not affect the characteristics of MB, it could transition to H_2O_2 catalyzed by NPs and generate •OH in the presence of Mn^{2+}, which could further oxidize MB. Hence, the feasibility of cascade reaction of glucose to H_2O_2 to •OH was validated, and the therapeutic potential of GOx@MnS NPs, a combination of H_2S donors and cascade catalysts, was also revealed.

Glucose-powered •OH generation with strong oxidation capacity is especially suitable for bacterial elimination in high-glucose condition. Two typical pathogenic bacteria strains, methicillin-resistant *Staphylococcus aureus* (MRSA, American Type Culture Collection (ATCC) 43300), and *Escherichia coli* (E. coli, ATCC 25922), were selected to demonstrate the bactericidal activity of GOx@MnS NPs. First, the typical dilution-plate counting method was adopted to explore the influence of concentration of NPs on its antibacterial effect. Around 10^8 colony formation unit (CFU) / mL of MRSA or *E. coli* was co-incubated with different concentrations of NPs (0, 2, 4, 8, 16, and 32 μg / mL) for 4 h in saline containing 10 mM glucose. As shown in Figure 3A and Figure 3C, GOx@MnS NPs exhibited a concentration-dependent but broad-spectrum bacterial killing property. In the case of MRSA, GOx@MnS NPs could induce the reduction of live bacteria at a low concentration (8 μg / mL). And the bactericidal rate rapidly elevated to ~99.6 % (from 9.3×10^8 CFU / mL to 4.0×10^6 CFU / mL) when the NPs concentration was doubled to 16 μg / mL. Further increased to 32 μg / mL, the bactericidal rate would exceed 99.99 % (from 9.3×10^8 CFU / mL to 1.9×10^4 CFU / mL), indicating that the minimum bactericidal concentration (MBC, generally identified as the minimum concentration of antibacterial agents for killing 99.9 % of the live bacteria) was slight over 16

μg / mL. The similar but more prominent results were obtained from *E. coli* group. Significant bacteria inhibition property was observed at a lower concentration (i.e., 4 μg / mL), and the MBC against *E. coli* was exactly 16 μg / mL (from 2.1×10^9 CFU / mL to 2.3×10^6 CFU / mL). This slight difference might be caused by the diverse cytoderm structure of these two pathogens. As a gram positive, multi-drug resistant bacteria strain, MRSA possesses a thicker and more compact cytoderm consisted of peptidoglycan compared with that of *E. coli*.[21] This structural difference enabled MRSA to be more resistant to exogenous oxidants.

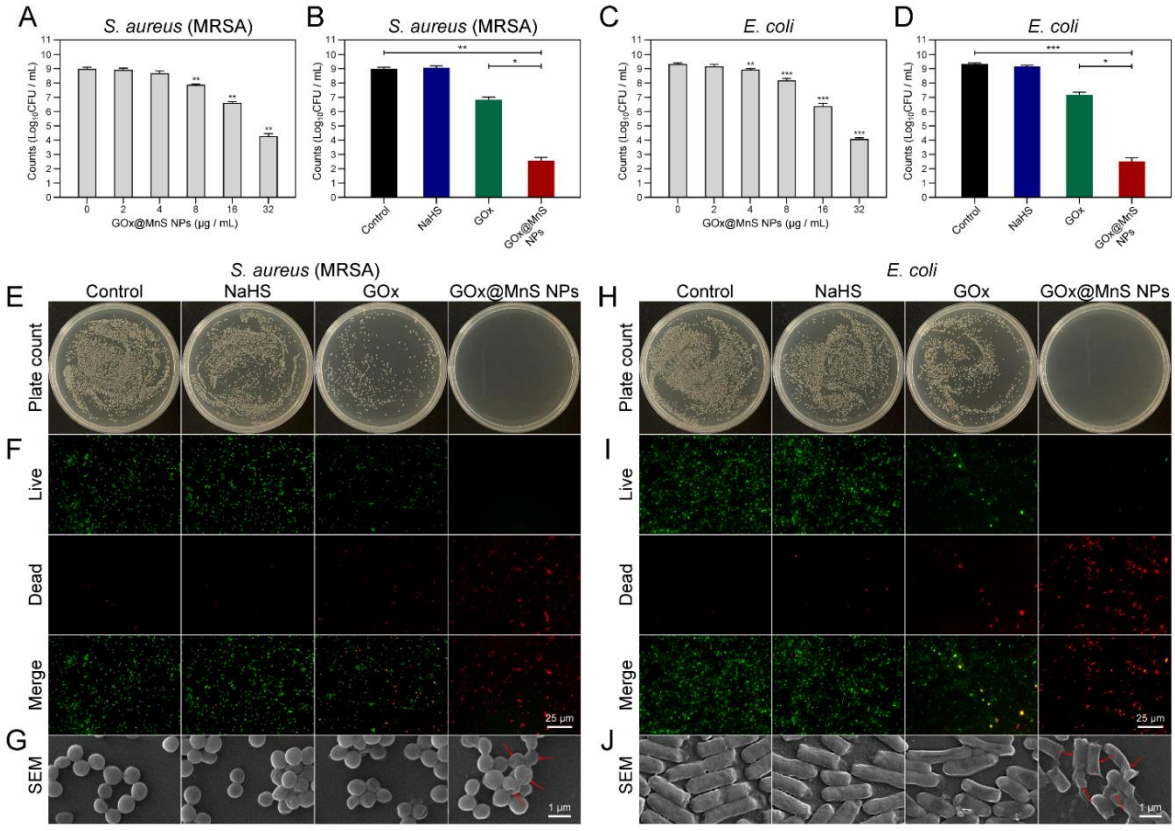

Figure 3. Bactericidal activities of GOx@MnS NPs against MRSA and *E. coli*. (A) MRSA and (C) *E. coli* treated with GOx@MnS NPs at different concentrations for 4 h in saline containing 10 mM glucose. (B) MRSA and (D) *E. coli* treated with NaHS, GOx or GOx@MnS NPs for 4 h in saline containing 10 mM glucose. (E) Agar plate counting of MRSA and (H) *E. coli* treated with NaHS, GOx or GOx@MnS NPs for 4 h in saline containing 10 mM glucose. (F) Live / dead fluorescent staining assay of MRSA and (I) *E. coli* treated with NaHS, GOx or GOx@MnS NPs for 4 h in saline containing 10 mM glucose. (G) Representative SEM images of MRSA and (J) *E. coli* treated with NaHS, GOx or GOx@MnS NPs for 4 h in saline containing 10 mM

glucose. Red arrows represent distorted bacteria. * $P < 0.05$, ** $P < 0.01$, *** $P < 0.001$, analyzed by Student's t-test. The concentration of NaHS was 100 μM, GOx was 25 μg / mL, and GOx@MnS NPs was 50 μg / mL used for B, D, E-J.

The comparison of therapeutic efficacy among GOx@MnS NPs and its main components, sulfide species and GOx, was then carefully examined following the same strategy. As we all know, H_2S is cytotoxic at high concentrations, but the effect at low concentrations (i.e., < 100 μM, referred to H_2S release kinetics of GOx@MnS NPs in Figure 2A) on bacteria remains elusive. GOx also confronted the similar problem that whether the low concentration of generated H_2O_2 is toxic enough to eradicate the bacteria. As demonstrated in Figure 3B and Figure 3D, H_2S (sourced from NaHS) at low concentrations showed no influence on bacteria while GOx exhibited its bactericidal activity through H_2O_2 generation. Notably, when combined together, GOx@MnS NPs showed the most significant inhibition effect (Figure 3B and Figure 3E for MRSA; Figure 3D and Figure 3H for *E. coli*). The live / dead fluorescent staining assay provided similar results (Figure 3F and Figure 3I). Specifically, almost all of the bacteria were alive and stained green after NaHS treatment while they were dead and stained red after NPs treatment. Interestingly, only a small portion of bacteria was stained red after treated with GOx. It may be because H_2O_2 suppressed the activity of some bacteria but did not directly kill them, and these suppressed bacteria could still be stained green. Then scanning electron microscope (SEM) was applied to visualize the morphological change after different treatments. As displayed in Figure 3G and Figure 3J, unlike control groups, the bacteria treated with NPs had some cracks and the surface shrunk to some extent. The oxidization-induced cytoderm destruction was then further verified by monitoring the protein leakage from bacteria cells. As for GOx@MnS NPs treated bacteria, concentrations of leaked protein in culture supernatant reached ~1.9 mg / mL, whereas the value of GOx treated ones was almost three times lower, i.e., only ~0.6 mg / mL (Figure S11). Moreover, the protein leakage was also confirmed by the activity of residual β-galactosidase inside the bacteria cells. *O*-nitrophenyl-β-*D*-galactoside (ONPG) was chosen as the indicator because it could freely permeate into the bacteria cells and unleash yellow nitrophenol after hydrolyzed by intracellular β-galactosidase.

Obviously, compared with control group or NaHS-treated group, bacteria treated by GOx or GOx@MnS NPs showed compromised β-galactosidase activities, with GOx@MnS NPs-treated group showing lower activity (Figure S12). Collectively, these results demonstrated the strong and broad-spectrum bactericidal capability of GOx@MnS NPs via cytoderm destruction in high-glucose conditions. More importantly, benefiting from powerful cascade reaction, GOx@MnS NPs could exert their efficacy at an extremely low concentration and avoid potential harmful side effects to normal tissues.

When infection occurs, bacteria adhered on the wound surface tend to secrete some mucopolysaccharides. These excretions would stick the bacteria together to form a dense film-like structure called biofilm.[22] Biofilm provides a shield for bacteria and makes them resistant to antibiotics or other antibacterial agents. In this regard, antibacterial materials capable of penetrating or breaking the biofilm would be useful for bacteria clearance and wound treatments. Herein, approximate 10^6 CFU / mL of MRSA or *E. coli* were statically cultured in high-glucose medium for 48 h to form mature biofilms respectively. Then, the biofilms were gently washed to remove floating bacteria on the surface. Same treatments aforementioned (co-incubation with NaHS, GOx or GOx@MnS NPs for 4 h in saline containing 10 mM glucose) were then applied to the biofilms and assessed whether the cascade reaction was still effective to enfolded bacteria within biofilms. Through crystal violet staining, MRSA biofilm treated with saline or NaHS could still be stained with dark purple, indicating that the structure remained intact. In case of GOx treated group, it seemed that the treatment could slightly reduce the thickness. Strikingly, GOx@MnS NPs treatment exhibited the most distinct outcome, in which the biomass was sharply declined (lighter purple) and the structure became partly tattered (Figure 4A). Due to the lack of intrinsic biofilm-formation ability, *E. coli* could only generate a thin and incompact biofilm. However, the therapeutic effects of different treatments on biofilms were still observable and followed the same trend (Figure 4D). It should be noted that the results of crystal violet staining were not convincing enough to judge the bactericidal capacity of different treatments against biofilms, because crystal violet stained all the bacteria cells sticked on the biofilm regardless of live or dead. To investigate whether GOx@MnS NPs could kill the

bacteria firmly sticked on the surface, three-dimensional (3D) reconstructions of treated groups, but red fluorescence was gloomy. It suggested that most of bacteria were still alive. In contrast, GOx@MnS NPs treated groups displayed entirely different results, i.e., the majority of biofilms became distorted and shriveled, and almost all the bacteria were dead and stained red even if they still adhered on the surface of culture dishes via residual biofilms (Figure 4B and Figure 4E). SEM images further validated the effect of GOx@MnS NPs on lowering the density of biofilms. Although extracellular mucopolysaccharide could not be directly observed by SEM, coherent bacteria cells on the surface still reflected the state of biofilms (Figure 4C and Figure 4F). Compared with control and NaHS treated groups, GOx@MnS NPs treatment significantly destroyed the dense arrangement of biofilms with some scattered bacteria left, which was consistent with the crystal violet staining and fluorescence results. Thus, we could deduce that the bactericidal activity of GOx@MnS NPs powered by cascade reaction remained effective to the bacteria embedded in biofilms.

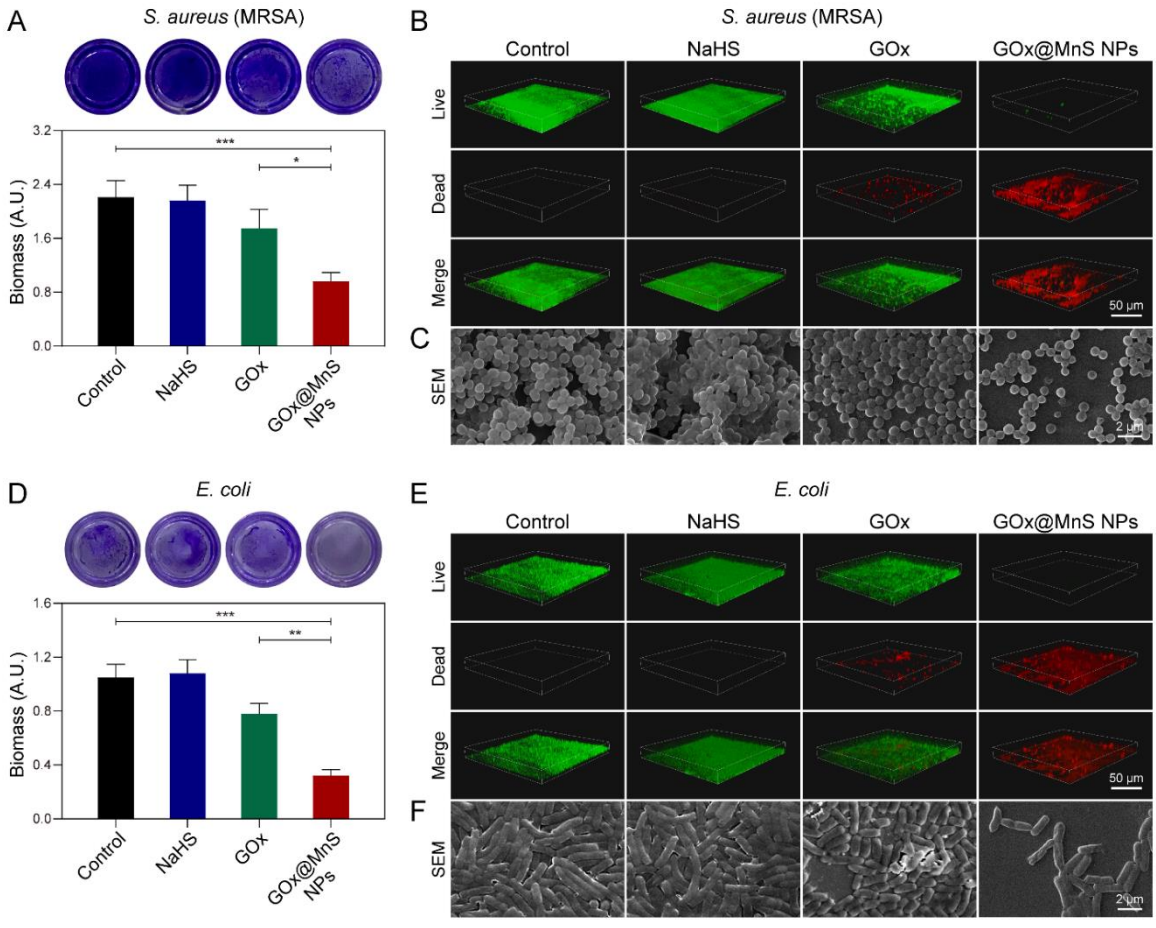

Figure 4. Anti-biofilm property of GOx@MnS NPs. (A) Crystal violet staining of MRSA and (D) *E. coli* biofilms treated with NaHS, GOx, or GOx@MnS NPs for 4 h in saline containing 10 mM glucose. (B) 3D CLSM images of MRSA and (E) *E. coli* biofilms treated with NaHS, GOx, or GOx@MnS NPs for 4 h in saline containing 10 mM glucose. The biofilms were stained with live / dead fluorescent dyes. (C) Representative SEM images of MRSA and (F) *E. coli* biofilms treated with NaHS, GOx, or GOx@MnS NPs for 4 h in saline containing 10 mM glucose. The concentration of NaHS was 100 μM, GOx was 25 μg / mL, and GOx@MnS NPs was 50 μg / mL. * $P < 0.05$, ** $P < 0.01$, *** $P < 0.001$, analyzed by Student's t-test.

Apart from antibacterial capability, the effect of GOx@MnS NPs as an immunomodulator was also explored. For *in vitro* tests, mouse macrophage cell line RAW264.7 and human umbilical vein endothelial cell line HUVEC were selected as models. Initially, biocompatibility of GOx@MnS NPs to both cell lines was evaluated. The results showed that GOx@MnS NPs were basically benign to RAW264.7 cells at all concentrations while non-toxic to HUVEC cells at low concentrations (Figure S13). In addition, the electronegative GOx@MnS NPs exhibited extremely weak hemolysis (Figure S14), demonstrating that GOx@MnS NPs were biocompatible and could be used for wound treatments. Native RAW264.7 cells are quiescent but can be easily activated to pro-inflammatory M1 phenotype when stimulated by pathogenic factors such as lipopolysaccharide (LPS).[23] So pre-treatment with 100 ng / mL of LPS was used to obtain M1 macrophages. After M1 induction and then treatment with NaHS or GOx@MnS NPs for 24 h, the expression of both Cluster of Differentiation 86 (CD86, M1 phenotype marker) and CD206 (M2 phenotype marker) were checked. CD206 immunofluorescent staining indicated that CD206 level was extremely low in native and M1 type macrophages, but the expression was upgraded after NaHS or GOx@MnS NPs treatment (Figure 5A). To provide the quantitative results, CD86 / CD206 double-labeling flow cytometry was carried out. It was found that the ratio of M1 macrophage ($CD86^{high}$ / $CD206^{low}$) increased from 4.97 % to 19.5 % after LPS pre-treatment, whereas this ratio decreased to 6.29 % and 6.97 % if LPS-induced macrophages were further treated with NaHS and GOx@MnS NPs, respectively. On the contrary, ratio of M2 macrophage ($CD86^{low}$ / $CD206^{high}$) lifted from 4.65 %

to 23.6 % and 24.2 % under the same condition (Figure 5B). Thus, both NaHS and GOx@MnS NPs were capable of inducing macrophage M2 polarization due to their H_2S releasing properties. Apparently, both NaHS and GOx@MnS NPs treatments could remarkably enhance the intracellular H_2S content in macrophages, but the effect of GOx@MnS NPs was better because of its prolonged H_2S release kinetics (Figure 5C).

To confirm the effect of M2 induction, several typical secreta of macrophages were detected. The expression of inducible nitric oxide synthase (iNOS) would be up-regulated when macrophages were induced to M1 type.[24] Therefore, the catalysate nitric oxide (NO) in the culture medium was tested using Griess assay. As showed in Figure 5D, M1 macrophages induced by LPS generated a high concentration of NO (~12 μM), while M2 macrophages transforming from M1 types after being treated with NaHS or GOx@MnS NPs exhibited low amount of NO generation. In addition, two typical pro-inflammatory cytokines, tumor necrosis factor α (TNF-α) (Figure 5E) and interleukin-6 (IL-6) (Figure 5F), along with a typical anti-inflammatory cytokine, interleukin-10 (IL-10) (Figure 5G), were analyzed using enzyme-linked immunosorbent assay (ELISA). The expression of TNF-α and IL-6 followed the same trend as NO generation that M1 macrophages resulted in high expression and M2 macrophage induced by NaHS or GOx@MnS NPs showed down regulated expression, while the expression of IL-10 was opposite to them. Taken together, all these results mutually validated that GOx@MnS NPs exerted the immunomodulatory effect of inducing macrophage M2 polarization via H_2S release.

Subsequently, the effect of different types of macrophages on promoting cell migration was studied using the scratch test. HUVEC cells in the culture dishes were scratched and co-incubated with the culture medium of macrophages after different treatments. Shrunken scratches in NaHS and GOx@MnS NPs treated groups were found, depicting that the immunomodulatory effect of GOx@MnS NPs could consequentially promote the migration of endothelial cells (Figure S16). Hence, GOx@MnS NPs exhibited their potential for accelerating the wound healing and promoting tissue repair.

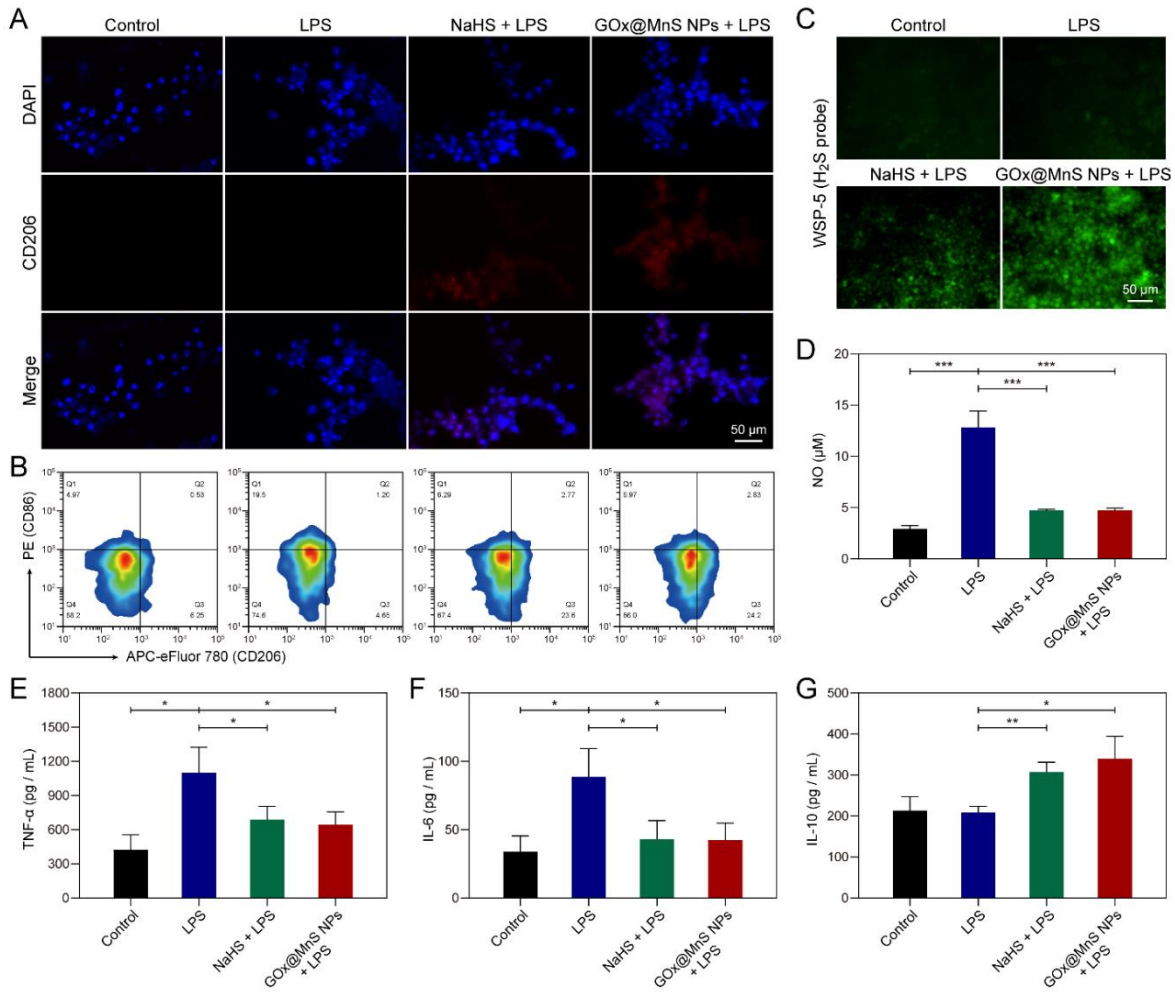

Figure 5. Immunomodulatory effect of GOx@MnS NPs on RAW264.7 cells. (A) CD206 immunofluorescent staining of RAW264.7 cells treated with LPS, LPS + NaHS, or LPS + GOx@MnS NPs for 24 h. (B) CD86 / CD206 flow cytometry of RAW264.7 cells treated with LPS, LPS + NaHS, or LPS + GOx@MnS NPs for 24 h. (C) Intracellular H_2S contents of RAW264.7 cells treated with LPS, LPS + NaHS, or LPS + GOx@MnS NPs for 6 h. WSP-5 was used as the probe. (D) NO concentration in culture medium of RAW264.7 cells treated with LPS, LPS + NaHS, or LPS + GOx@MnS NPs for 24 h. (E) TNF-α, (F) IL-6, and (G) IL-10 contents in culture medium of RAW264.7 cells treated with LPS, LPS + NaHS, or LPS + GOx@MnS NPs for 24 h quantified by ELISA. The concentration of LPS was 100 ng / mL, NaHS was 100 μM, and GOx@MnS NPs was 25 μg / mL. LPS here represents that the cells were pre-treated by LPS for 24 h to induce M1 phenotype before receiving other treatments. * $P < 0.05$, ** $P < 0.01$, *** $P < 0.001$, analyzed by Student's t-test.

Encouraged by excellent bactericidal activity as well as immunomodulatory effect of GOx@MnS NPs *in vitro*, further *in vivo* tests were performed to examine whether they were powerful for curing diabetic ulcer infection. Institute of cancer research (ICR) mice were firstly intraperitoneal injected with streptozocin to induce diabetes mellitus, then wounds of ~70 mm^2 were created on the back of the diabetic mice, followed by *in situ* infection of MRSA (~5×10^6 CFU). MRSA were allowed to grow on the wound surface for 1 day to ensure severe ulcer generation, then GOx@MnS NPs or other control reagents were spread on the wound surface at day 1 and day 3 (Figure 6A). The wounds were photographed and measured every other day. As revealed in Figure 6B, GOx@MnS NPs treated group showed a remarkably faster healing rate compared with other groups, where ulcer started to relieve at day 3 while other groups showed no obvious change at the same time. At day 5, all the wounds formed scabs, and the wound area treated with GOx + $MnCl_2$ group also started to shrink. The difference in healing rate between GOx + $MnCl_2$ treated group and GOx@MnS NPs treated one was probably because of the lack of H_2S to suppress inflammation and regenerate new tissues. All the wounds then gradually recovered over time, with GOx@MnS NPs and GOx + $MnCl_2$ treated groups exhibited a much fast healing rate. The average wound area of GOx@MnS NPs group decreased to around 12 mm^2 at day 11, while that of GOx + $MnCl_2$ group was approximate two times larger, reaching 25 mm^2 (Figure 6D). Although the combination of GOx and Mn^{2+} could also trigger the formation of •OH and effectively kill the infected bacteria (Figure 6C and Figure 6E), the lack of H_2S caused the delay of macrophage polarization and tissue regeneration. Hence, both cascade reaction of •OH formation and H_2S release were essential for the excellent therapeutic outcome of GOx@MnS NPs on clearing diabetic infection.

Histologic section analysis was then carried out (Figure 6F). The hematoxylin & eosin (H&E) staining indicated that the wound tissues in control, NaHS, and GOx groups still suffered from severe inflammatory macrophages and lymphocytes infiltration (denser cell nucleus and darker purple staining) at day 11. In contrast, tissue of GOx + $MnCl_2$ treated group exhibited better recovery condition without obvious inflammatory response. Notably, GOx@MnS NPs treated one provided the best healing effect: some neogenetic hair follicles appeared, and the general

state of the tissue was almost close to normal derma tissue. Masson staining also showed similar results, with GOx@MnS NPs and GOx + $MnCl_2$ groups exhibiting higher extents of collagen deposition. Moreover, the biocompatibility of GOx@MnS NPs was verified by monitoring changes of body weight (Figure S17) as well as H&E staining of main organs (Figure S18). These results demonstrated a healing wound with low inflammatory response, low infection level as well as satisfying tissue regeneration contributed by GOx@MnS NPs treatment, which was the direct evidence for the therapeutic potential of this nanomaterial.

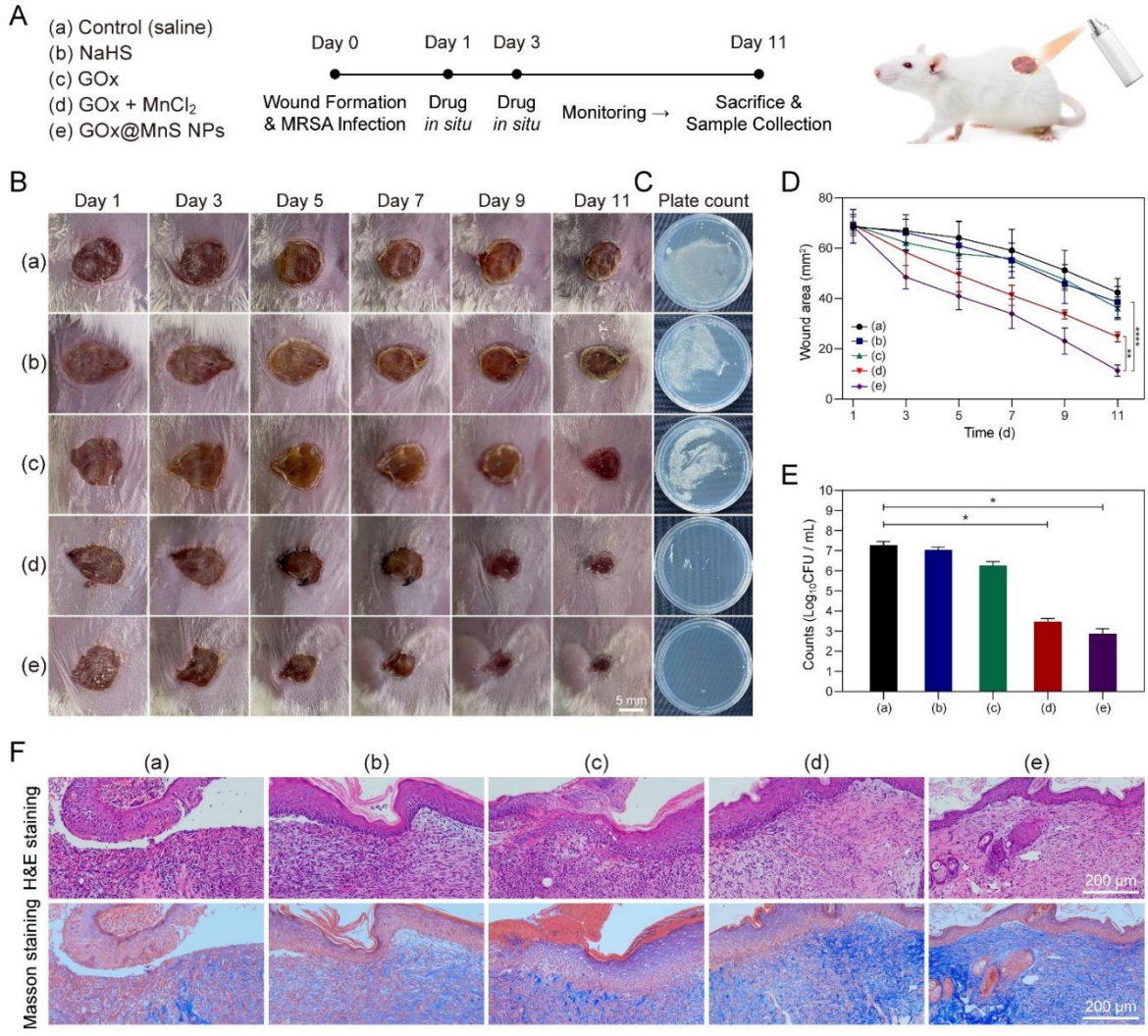

Figure 6. Therapeutic effects of GOx@MnS NPs on diabetic wound infection model. (A) Schematic diagram of model establishment and grouping information. (B) Images of wounds from day 1 to day 11. (C) Agar plate counting of residual bacteria in homogenized wound tissue suspensions. (D) Quantitative analysis of wound areas. (E) Concentration of residual bacteria

in homogenized wound tissue suspensions. (F) H&E staining and Masson staining of wound tissue sections. The concentration of NaHS was 100 μM, GOx was 25 μg / mL, $MnCl_2$ was 500 μM, and GOx@MnS NPs was 50 μg / mL. * $P < 0.05$, ** $P < 0.01$, **** $P < 0.0001$, analyzed by Student's t-test.

To make this conclusion more convincing, the immunomodulatory effect of GOx@MnS NPs was also assessed *in vivo*. CD31, a key biomarker of angiogenesis, was detected via immunofluorescent staining of derma tissues. CD31 expression was generally low in all groups compared with normal tissues because the wounds had not been completely healed. Nevertheless, the expression of this index in GOx@MnS NPs treated group was still significantly higher than those of other groups, indicating that the healing process was in the late stage. It was also consistent with CD206 staining results. Although the amount of infiltrated inflammatory cells was lower in GOx + $MnCl_2$ or GOx@MnS NPs treated groups (refer to DAPI staining or H&E staining above), CD206 expression in these two groups was much higher compared with those of other groups (Figure 7A), which meant that residual macrophages were mainly M2 phenotype for tissue regeneration. Moreover, the systemic inflammatory response caused by wound infection could also be effectively suppressed by GOx@MnS NPs treatment. Blood-related indexes, including white blood cells (WBCs) counting and plasma cytokine contents, corroborated the effect as well. Specifically, WBCs content of GOx + $MnCl_2$ and GOx@MnS NPs treated groups was remarkably lower than that of other groups, with GOx@MnS NPs treated group even lower than GOx + $MnCl_2$ treated one (Figure S19). In addition, content of pro-inflammatory cytokines (TNF-α and IL-6) in plasma followed the same tendency (Figure 7B and Figure 7C), whereas anti-inflammatory IL-10 was reverse (Figure 7D). Relying on these results, we could finally confirm the good performance of GOx@MnS NPs as an immunomodulatory agent.

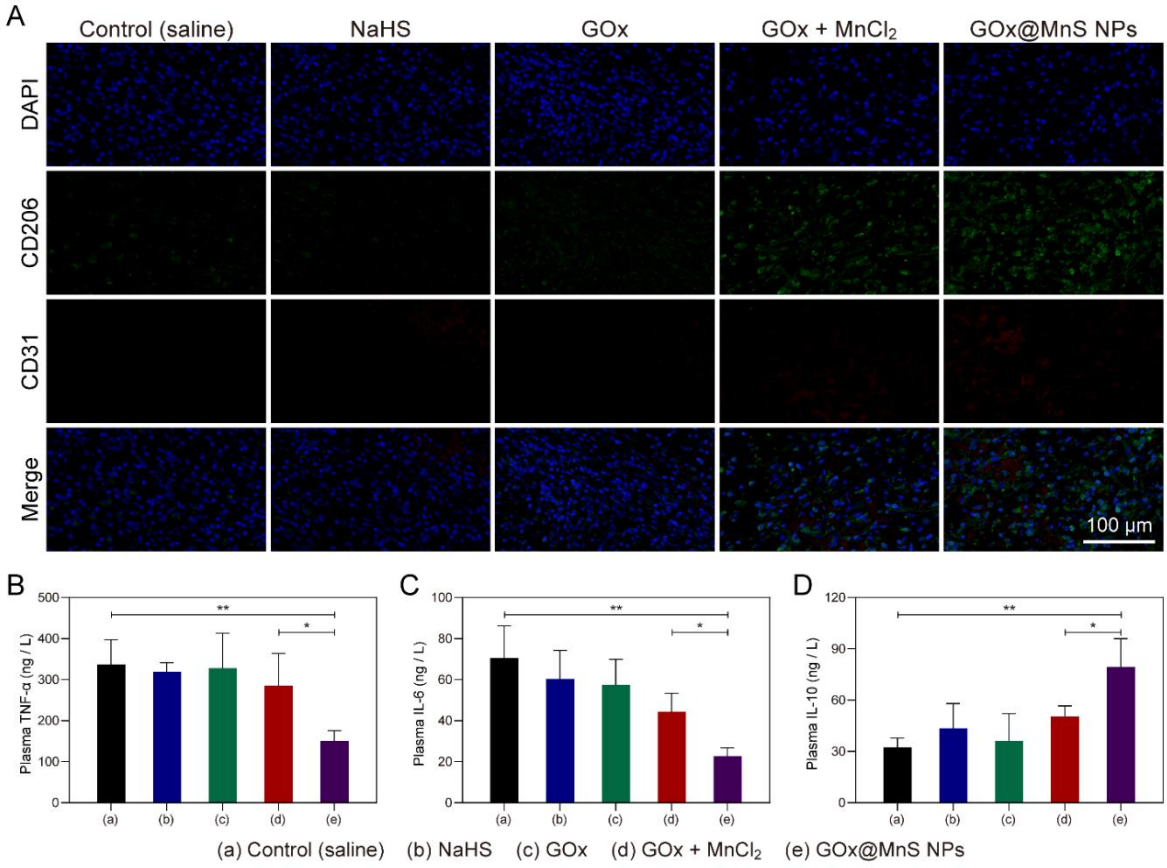

Figure 7. Angiogenesis and inflammation level of diabetic wound infection model. (A) CD31 (red) / CD206 (green) immunofluorescent staining of wound tissue sections. (B) Plasma TNF-α, (C) IL-6 and (D) IL-10 contents of diabetic mice at day 11 quantified by ELISA. * $P < 0.05$, ** $P < 0.01$, analyzed by Student's t-test.

3. Conclusion

In summary, we developed a dual-functional nanomaterial, GOx@MnS NPs, through a single-step *in situ* biomineralization for diabetic wound treatment. GOx worked as a template for MnS deposition during the synthetic procedure and also stabilized the resultant NPs in aqueous solution. As the catalytic activity of GOx was well preserved in NPs, it would allow NPs to effectively convert glucose to H_2O_2. Meanwhile, deposited MnS provided sustained and pH-responsive H_2S release as well as the catalyst for Mn^{2+}-mediated Fenton-like reaction. Powered by high-glucose level of diabetic wounds, GOx@MnS NPs would gradually decompose and initiate the glucose - H_2O_2 - •OH cascade reaction as well as H_2S release. Hence, the bactericidal activity by •OH and immunomodulatory effect through H_2S release could be simultaneously

achieved. In view of the stimuli-responsive drug release behavior, strong and broad-spectrum anti-bacterial capacity, remarkable anti-inflammatory capacity as well as good biocompatibility, this nanomaterial demonstrated its considerable therapeutic potential for diabetic infection treatment.

Supporting Information

Supporting Information is available from the Wiley Online Library or from the author.

Acknowledgements

Financial support from the National Natural Science Foundation of China (22105126), the Natural Science Foundation of Shanghai (22ZR1433500), the National Facility for Translational Medicine (Shanghai) (TMSK-2021-205), the Open Project Program of Engineering Research Center of Cell & Therapeutic Antibody, Ministry of Education, Shanghai Jiao Tong University（22X010201609-004）and startup funding from Shanghai Jiao Tong University is acknowledged. We also thank Dr. Bin Hao for his helpful discussion, and Dr. Weijiang Yu for his illustration drawing.

Conflict of Interests

The authors declare no conflict of interests.

Received: ((will be filled in by the editorial staff))

Revised: ((will be filled in by the editorial staff))

Published online: ((will be filled in by the editorial staff))

References

[1] Y. Zheng, S. H. Ley, F. B. Hu, *Nat. Rev. Endocrinol.* **2018**, *14*, 88-98.

[2] L. M. Frydrych, G. Bian, D. E. O'Lone, P. A. Ward, M. J. Delano, *J. Leukoc. Biol.* **2018**, *104*, 525-534.

[3] A. J. Boulton, L. Vileikyte, G. Ragnarson-Tennvall, J. Apelqvist, *Lancet* **2005**, *366*, 1719-1724.

[4] a) F. Du, J. Ma, H. Gong, R. Bista, P. Zha, Y. Ren, Y. Gao, D. Chen, X. Ran, C. Wang, *Front. Endocrinol.* **2022**, *13*, 881659; b) P. C. Matthews, A. R. Berendt, B. A. Lipsky, *Expert. Rev. Anti. Infect. Ther.* **2007**, *5*, 117-127.

[5] a) L. Gao, J. Cheng, Z. Shen, G. Zhang, S. Liu, J. Hu, *Angew. Chem. Int. Ed.* **2022**, *61*, e202112782; b) Y. Liang, M. Li, Y. Yang, L. Qiao, H. Xu, B. Guo, *ACS Nano* **2022**, *16*, 3194-3207.

[6] a) J. A. Bauer, M. Zamocka, J. Majtan, V. Bauerova-Hlinkova, *Biomolecules* **2022**, *12*; b) Y. Zhang, S. Jiang, J. Lin, P. Huang, *Angew. Chem. Int. Ed.* **2022**, *61*, e202208583.

[7] Y. Li, L. Su, Y. Zhang, Y. Liu, F. Huang, Y. Ren, Y. An, L. Shi, H. C. van der Mei, H. J. Busscher, *Adv. Sci.* **2022**, *9*, e2103485.

[8] Y. Zhang, L. Lai, Y. Liu, B. Chen, J. Yao, P. Zheng, Q. Pan, W. Zhu, *ACS Appl. Mater. Interfaces* **2022**, *14*, 6453-6464.

[9] L. Chen, S. Xing, Y. Lei, Q. Chen, Z. Zou, K. Quan, Z. Qing, J. Liu, R. Yang, *Angew. Chem. Int. Ed.* **2021**, *60*, 23534-23539.

[10] a) L. Chen, Y. Chen, R. Zhang, Q. Yu, Y. Liu, Y. Liu, *ACS Nano* **2022**, *16*, 9929-9937; b) Y. Z. Piao, Y. Qi, X. W. Hu, Y. Wang, Y. Li, T. Zhou, L. Shi, Y. Liu, C. Zhou, *J. Control. Release* **2022**, *352*, 1-14.

[11] a) Z. Shen, S. Zheng, S. Xiao, R. Shen, S. Liu, J. Hu, *Angew. Chem. Int. Ed.* **2021**, *60*, 20452-20460; b) D. Liu, Y. Liao, E. J. Cornel, M. Lv, T. Wu, X. Zhang, L. Fan, M. Sun, Y. Zhu, Z. Fan, J. Du, *Chem. Mater.* **2021**, *33*, 7972-7985; c) Z. Wang, F. Rong, Z. Li, W. Li, K. Kaur, Y. Wang, *Chem. Eng. J.* **2023**, *452*; d) W. Ma, X. Chen, L. Fu, J. Zhu, M. Fan, J. Chen, C. Yang, G. Yang, L. Wu, G. Mao, X. Yang, X. Mou, Z. Gu, X. Cai, *ACS Appl. Mater. Interfaces* **2020**, *12*, 22479-22491.

[12] a) Y. Ge, F. Rong, W. Li, Y. Wang, *J. Control. Release* **2022**, *352*, 586-599; b) F. Rong, T. Wang, Q. Zhou, H. Peng, J. Yang, Q. Fan, P. Li, *Bioact. Mater.* **2023**, *19*, 198-216.

[13] G. Rayman, A. N. Lumb, B. Kennon, C. Cottrell, D. Nagi, E. Page, D. Voigt, H. C. Courtney, H. Atkins, K. Higgins, J. Platts, K. Dhatariya, M. Patel, P. Newland-Jones, P. Narendran, P. Kar, O. Burr, S. Thomas, R. Stewart, *Diabet. Med.* **2021**, *38*, e14378.

[14] a) C. R. Powell, K. M. Dillon, J. B. Matson, *Biochem. Pharmacol.* **2018**, *149*, 110-123; b) Y. Wang, Z. Li, Y. Shmidov, R. J. Carrazzone, R. Bitton, J. B. Matson, *J. Am. Chem. Soc.* **2020**, *142*, 20058-20065; c) J. Li, L. Xie, B. Li, C. Yin, G. Wang, W. Sang, W. Li, H. Tian, Z. Zhang, X. Zhang, Q. Fan, Y. Dai, *Adv. Mater.* **2021**, *33*, e2008481.

[15] a) T. He, X. Qin, C. Jiang, D. Jiang, S. Lei, J. Lin, W. G. Zhu, J. Qu, P. Huang, *Theranostics* **2020**, *10*, 2453-2462; b) C. Xie, D. Cen, Z. Ren, Y. Wang, Y. Wu, X. Li, G. Han, X. Cai, *Adv. Sci.* **2020**, *7*, 1903512; c) D. Cen, Q. Ge, C. Xie, Q. Zheng, J. Guo, Y. Zhang, Y. Wang, X. Li, Z. Gu, X. Cai, *Adv. Mater.* **2021**, e2104037.

[16] L. H. Fu, Y. R. Hu, C. Qi, T. He, S. Jiang, C. Jiang, J. He, J. Qu, J. Lin, P. Huang, *ACS Nano* **2019**, *13*, 13985-13994.

[17] Z. Tang, Y. Liu, M. He, W. Bu, *Angew. Chem. Int. Ed.* **2019**, *58*, 946-956.

[18] S. Hayashi, S. Nakamura, *Biochim. Biophys. Acta* **1981**, *657*, 40-51.

[19] C. M. Wong, K. H. Wong, X. D. Chen, *Appl. Microbiol. Biotechnol.* **2008**, *78*, 927-938.

[20] F. M. Boubeta, S. A. Bieza, M. Bringas, J. C. Palermo, L. Boechi, D. A. Estrin, S. E. Bari, *Antioxid. Redox Signal.* **2020**, *32*, 247-257.

[21] D. A. Dik, J. F. Fisher, S. Mobashery, *Chem. Rev.* **2018**, *118*, 5952-5984.

[22] J. W. Costerton, P. S. Stewart, E. P. Greenberg, *Science* **1999**, *284*, 1318-1322.
[23] D. Zhou, C. Huang, Z. Lin, S. Zhan, L. Kong, C. Fang, J. Li, *Cell. Signal.* **2014**, *26*, 192-197.
[24] H. Cho, H. Y. Kwon, A. Sharma, S. H. Lee, X. Liu, N. Miyamoto, J. J. Kim, S. H. Im, N. Y. Kang, Y. T. Chang, *Nat. Commun.* **2022**, *13*, 5974.

Table of Contents (ToC)

Hydrogen sulfide-releasing nanocascade templated by glucose oxidase for diabetic infection treatment

*Yuxuan Ge, Fan Rong, Yujia Lu, Zixin Wang, Jinyu Liu, Junsheng Chen, Wei Li, and Yin Wang**

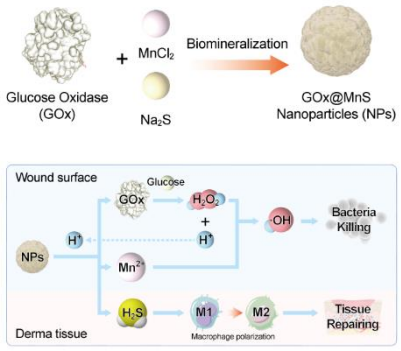

Biomineralization of glucose oxidase (GOx) and manganese sulfide (MnS) was established to construct a nanocascade, GOx@MnS nanoparticles (NPs). Activated by glucose, the NPs could generate hydroxyl radicals (•OH) to kill bacterial and release hydrogen sulfide (H_2S) to induce macrophage polarization and accelerate the tissue regeneration, which provided great therapeutic potential for diabetic infection treatment.